Plasma flow control of the tip vortices over a very low aspect-ratio wing

Lei Dong (董磊),[1] Kwing-So Choi,[1,a)] Yaxing Wang (王亚兴)[1]

AFFILIATIONS

[1]Faculty of Engineering, University of Nottingham, Nottingham NG7 2RD, UK

[a)]**Author to whom correspondence should be addressed:** kwing-so.choi@nottingham.ac.uk

ABSTRACT

Flow control of the tip vortices over a very low aspect-ratio wing was carried out using the dielectric-barrier-discharge plasma actuators. The results indicate a large change in the aerodynamic forces by plasma flow control, where the lift coefficient is increased by the blowing plasma actuator by 23%, and is reduced by the suction plasma actuator by 30%. The change of the drag coefficient is less than 10%. The blowing plasma moves the tip vortex outboard away from the wing tip, increasing the streamwise vorticity as well as the turbulence intensities and the Reynolds stress. With the suction plasma, the tip vortex is shifted inboard closer to the wing tip. Co-flowing with the tip vortex, the blowing plasma increases the tip vortex circulation, while it is reduced by the counter-flowing suction plasma.

I. INTRODUCTION

The aerodynamics of a low aspect ratio (AR) wing is fundamentally different from a two-dimensional (2D) aerofoil. It was demonstrated (Winkelman and Barlow, 1980 and Freymuth *et al.*, 1988) that low AR wings are dominated by a leading-edge vortex (LEV) with a pair of tip vortices (TVs). Here, the formation of the TVs is attributed to the pressure difference between the pressure and suction sides of the wing (Green 1995). In other words, the flow near the wing tip is pulled outboard and moves towards the suction side of the wing, forming the streamwise vortices known as the TVs. The existence of the TVs influences the behaviour of the leading-edge flow (DeVoria and Mohseni, 2017 and Dong *et al.*, 2020), promoting the formation of the recirculation area near the leading edge of the wing. Besides, the interaction of these vortices influences the flow field over the wing body, creating a three-dimensional (3D), complex wake region (Taira and Colonius, 2009).

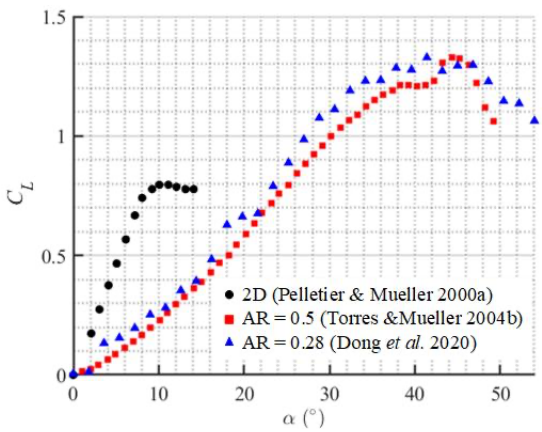

Fig. 1 Comparison of the lift coefficient C_L between the 2D aerofoil and the very-low AR wings.

The existence of the TVs over a low AR wing leads to a significantly different lift curve as compared to that of the 2D aerofoil, see Fig. 1. Although the lift slope of the low AR wing is very small at small angles of attack (AoA), it increases with an increase in the AoA. As a result, the lift coefficient C_L of a low AR wing eventually reaches to more than 1.5 times that of the 2D aerofoil at $\alpha = 45°$. It was shown (Torres and Mueller, 2004 and Taira and Colonius, 2009) that the maximum lift angle of the wing is further increased with a reduction in the AR. For low AR wings, the total lift on the wing is a combination of the spanwise circulation of the LEV through the Kutta-Joukowski theorem and the pressure force of the TVs (i.e., the vortex lift). The development of the LEV, however, is influenced by velocity induction of the TVs due to the Biot-Savart law (Harbig *et al.*, 2013 and Dong *et al.*, 2022). The interaction between the LEV and the TVs was studied by

Dong *et al.* (2020 and 2022) who demonstrated that the reattachment of the leading-edge flow and the subsequent formation of the LEV were strongly influenced by the TVs. They also observed that the size and strength of the TVs were increased with an increase in the AoA. By correlating the aerodynamic forces with the vortical structures along the span of the NACA 0015 wing, the sectional lift force exhibited considerable fluctuations close to the mid-span and maintained a relatively steady value at the wing tip, suggesting that the TVs could stabilise the unsteady LEV shedding (Zhang *et al.*, 2020). At a very low AR (AR < 1), the leading-edge separated flow formed a large separation bubble with strong recirculated velocities in the vicinity of the leading edge due to the downwash induced by the TVs, reducing the amount of the vorticity shedding downstream, which consequently strengthened the bound vortex and generated a high lift force (DeVoria and Mohseni, 2017).

The dielectric-barrier-discharge (DBD) plasma actuators are composed of two electrodes separated by a thin dielectric sheet. When they are excited by high AC voltage at high frequencies, the air in the vicinity of the exposed electrode is weakly ionised, generating an ionic jet. This couples the momentum of the air flow, which can be used for flow control. DBD plasma flow control has unique advantages over the conventional control devices, since the DBD plasma actuators are fast response with no moving parts involved (i.e., all electric devices) which can be retrofitted to the aerodynamic bodies. Historical background on DBD plasma actuators and their applications to aerodynamics are given by Moreau (2007), Corke *et al.* (2010), Wang *et al.* (2013), Choi *et al.* (2015) and Kriegseis *et al.* (2016).

The influence of the plasma on the aerodynamic forces on a NACA 0009 aerofoil was investigated by Corke *et al.* (2002), where both the lift and drag coefficients were increased using a DBD plasma actuator. They concluded that one of the functions of the plasma actuator was to increase the camber of the aerofoil. The leading-edge flow separation was also controlled by the plasma actuator, resulting in a significant reduction in the wake area (Roth, 2003). As a result, the stall angle of the aerofoil was delayed by up to 8º with an improved lift-to-drag ratio (Post and Corke, 2004). Vorobiev *et al.* (2008) examined the effectiveness of plasma control on an aerofoil at different Reynolds numbers, showing that the lift coefficient was enhanced by up to 30% by the plasma actuator. However, this lift enhancement by the plasma actuator became weaker with an increase in the Reynolds number. It was demonstrated that the plasma actuator affected the aerodynamics of the wing in two ways -- adding momentum to the flow and suppressing viscous effect in the vicinity of the trailing edge. He *et al.* (2009) and Feng *et al.* (2015) studied the impact of the plasma actuator placed at the trailing edge of the aerofoil, showing that the plasma actuator could behave as a virtual Gurney flap.

Apart from the leading-edge and trailing-edge flow control, the plasma actuator was also placed close to the wing tip to modify the TVs. Hasebe *et al.* (2011) investigated the effect of the blowing and suction plasma actuators on the TVs of a NACA 0012 wing with an AR of 0.5, showing that the strength of the TVs was suppressed by both plasma actuators, leading to a lower lift-to-drag ratio. Boesch *et al.* (2010) also studied the influence of the blowing plasma actuator on the TVs of a NACA 4418 (AR = 2). They, however, concluded that the TVs became diffusive and moved outboard with plasma on, which in turn mitigated the influence of the downwash to give a high lift. Plasma control of the TVs over the delta wing was conducted by Shen and Wen (2017) who symmetrically placed the suction plasma actuator on both leading edges of a slender delta wing to modify the TVs. The separated shear layer at the wing tip was pulled towards the wing surface by the DBD plasma actuator, influencing the structure of the TVs. In particular, the TV breakdown was delayed by the symmetrical control but promoted by the asymmetrical control. The aerodynamic forces of this delta wing, however, did not exhibit any changes. Greenblatt *et al.* (2008) used the pulsed suction DBD plasma actuator to modify the TVs on a delta wing after the vortex breakdown. They found that the breakdown of the TVs was delayed under the influence of the plasma actuator, resulting in a significant increase in the lift. Similar results were also mentioned by Sidorenko *et al.* (2013) but their optimum modulation frequency of the plasma actuator was twice larger than that of Greenblatt *et al.* (2008).

Previously, we have studied the interaction between the TVs and the LEV over a stationary and pitching very low AR wing, where the influence of the TVs on the development of the LEV was demonstrated (Dong *et al.*, 2020 and 2022). Building on the understanding of the vortex interactions gained from these studies, a flow control study of a very low AR wing was carried out using DBD plasma actuators. By controlling the TVs using the plasma jet at the wing tip, we were able to influence the aerodynamic forces of the wing. The influence of the plasma actuators on the TVs was analysed by documenting the vortex locus as well as velocity and vorticity distributions around the vortex core to understand the mechanism of plasma control of a very low AR wing.

II. EXPERIMENTAL SET-UP

An experimental study was conducted in a low-speed, open-return wind tunnel (Fig. 2a) with a test section of 1.5 m × 0.9 m × 0.8 m (length × width × height) at the University of Nottingham (Kim *et al.*, 2022), where the port side of the TV of a very-low AR wing was controlled by the plasma actuators to modify the aerodynamic characteristics. The freestream velocity U_∞ of the wind tunnel was set at 10 m/s, which was monitored by a Pitot tube placed 0.2 m downstream of the contraction section. The wing model was manufactured from a 3-mm thick aluminium composite flat plate, which had a chord length of c = 260 mm and a half span length of s = 36 mm, corresponding to a very low aspect-ratio of 0.277

with a thickness-to-chord ratio of 1.2%, see Fig. 3. A 3D-printed elliptic leading edge (18 mm of major axis and 3 mm of minor axis) was attached. The maximum blockage of the wind tunnel due to the wing model was 1.8% at $\alpha = 90°$. The wing model, whose chord Reynolds number is 2×10^5, was placed in the centre of the wind-tunnel test section where the freestream turbulence intensity was 0.3%. After installing a turbulence-generating grid 0.5 m upstream of the wing model, the turbulence intensity in the freestream was increased to 4%. This has increased the effective Reynolds number to 3×10^6 by promoting transition to turbulence near the leading edge of the wing. Here, the effective Reynolds number is the equivalent Reynolds number in the aerodynamic tests where the freestream turbulence level is nearly zero (Wang *et al.* 2014). The use of turbulence-generating grid was to remove the ambiguity in aerodynamic measurements at low to medium Reynolds numbers, where the aerodynamic forces on wings are influenced by the boundary-layer transition (Mueller, 1985). Figure 2b shows the laboratory-based coordinate system used in the present study, where x, y and z denote the streamwise, cross-flow and spanwise directions, respectively, corresponding to their mean velocity components U, V and W and fluctuation velocities u, v and w.

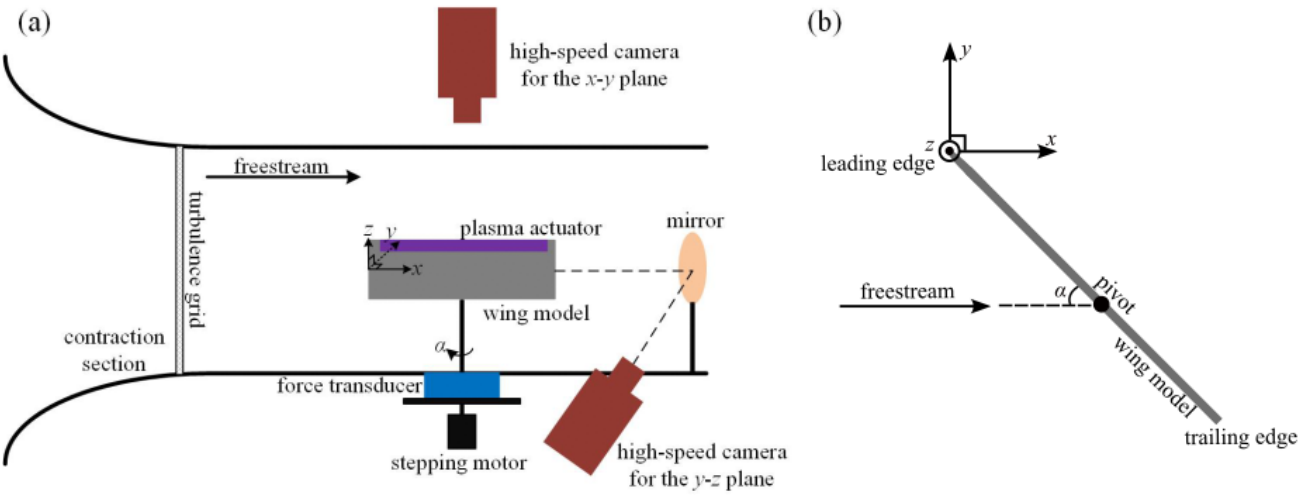

Fig. 2 (a) Schematic of the experimental set-up in the wind tunnel and (b) the coordinate system for the plan view.

The plasma actuators were placed only one side of the wing model, see Fig. 3, where two different configurations of plasma actuators were considered. The first plasma configuration was intended to blow a synthetic plasma jet away from the wing tip, while the second plasma configuration was intended to draw the air from the wing tip. They were called the blowing and suction plasma actuators, respectively. Both plasma actuators consisted of an upper exposed electrode and a lower encapsulated electrode made of a single layer of 0.05-mm thick and 240-mm long copper tapes, separated by two layers of 0.15-mm thick Cirlex sheets. For the blowing plasma actuator, a pair of 10-mm wide upper electrodes was attached 10 mm from the wing tip as shown in Fig. 3a. For the suction plasma actuator, on the other hand, a 3-mm wide upper electrode was attached over the tip edge of the wing, see Fig. 3b. The Reynolds number based on the thickness of the plasma actuators and the freestream velocity was $Re_p = 270$, which was below the critical Reynolds number for triggering boundary-layer transition (Schlichting 1955). Therefore, the roughness effect of the model wing due to the plasma actuators was negligible. Plasma actuators were excited with a sinusoidal waveform by a Minipuls 6 AC power supply at a peak-to-peak voltage E_{PP} = 18 kV and an operating frequency of 7 kHz. The plasma power cables were taken out through the bottom floor of the wind tunnel from the trailing edge of the wing model.

The wing model was mounted on a Kyowa LSM-B-SA1 three-component force transducer for aerodynamic force measurements via a 150-mm long strut to avoid the boundary layer over the wind tunnel floor, see Fig. 2. This transducer was rated at 10 N in all three components with an absolute accuracy of ±0.02 N. The measured signals from the force transducer were amplified and low-pass filtered by a Kyowa DPM-911B strain-gauge amplifier with a cut-off frequency of 100 Hz before being sent to a NI 9215 16-bit analogue-to-digital converter on a NI CompactRIO system. The AoA of the wing was controlled by a step motor driven by a NI 9512 driver, giving a minimum step angle of 0.1°. Force measurements were repeated 50 times at a sampling rate of 2000 Hz from $\alpha = 0°$ to $\alpha = 90°$ with an interval of 1.8°, each of which lasted 3 s with plasma off followed by 3 s with plasma on. The performance of plasma flow control during the "plasma on" period was evaluated against the "plasma off" condition throughout this study. The lift force F_L and drag force F_D of the wing model were calculated by $F_L = F_N \cos\alpha - F_A \sin\alpha$ and $F_D = F_N \sin\alpha + F_A \cos\alpha$, respectively, from the measured normal force F_N and the axial force F_A. The lift and drag coefficients were given by $C_L = F_L/\frac{1}{2}\rho U_\infty^2 A$ and $C_D = F_D/\frac{1}{2}\rho U_\infty^2 A$, where ρ is the air density, U_∞ is the freestream velocity and A is the plan area of the wing.

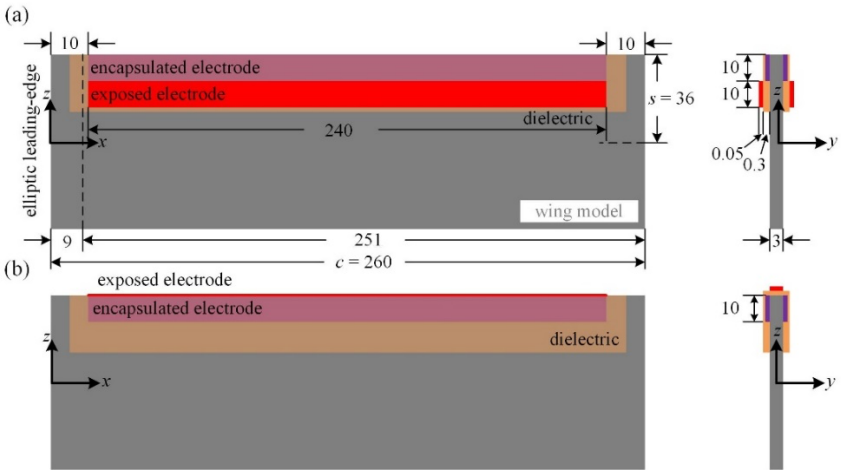

Fig. 3 Configuration of the plasma actuator on the very low AR wing: (a) blowing plasma actuator and (b) suction plasma actuator. All dimensions are in millimetre.

Tab. 1 Momentum coefficient of different plasma actuators

f^+	0	2
C_μ (blowing plasma actuators)	0.4%	0.27%
C_μ (suction plasma actuators)	0.32%	0.21%

The flow field over the wing was measured using a fast-speed, two-dimensional particle image velocimetry (PIV) system by Dantec on the *x-y* plane and *y-z* plane, as shown in Fig. 2. Two seeding generators (TSI 9307-7) were placed upstream of the contraction section of the wind tunnel to create uniformly distributed tracer particles with a diameter of approximately 1 μm. A Litron LDY 302-PIV Nd:YLF dual-cavity laser with 15 mJ per pulse was used to generate a thin laser light sheet, where the particle images were captured with a CMOS high-speed camera at a resolution of 1280 × 800 pixels. We used a 110 mm Canon lens in the *x-y* plane and a 200 mm Canon lens in the *y-z* plane, where the corresponding field of view was $0.55c \times 0.35c$ and $2s \times 1.5s$, respectively. In the *x-y* plane measurement, the laser light sheet with a thickness of 0.5 mm was set parallel to the freestream from $z = 0$ to $z = 2s$ in $0.11s$ increments, where the time delay between the laser pulses was set to 50 μs. To minimise the measurement error due to out-of-plane motion of seeding particles, the laser sheet thickness was increased to 2 mm and the time interval between laser pulses was reduced to 30 μs in the *y-z* plane measurement. To allow the camera to be set outside the wind tunnel for the *y-z* plane measurements, a 100 mm diametral mirror was mounted on the wind tunnel floor, 300 mm downstream the model at 45° to the freestream. Here, 14 planes were investigated from the leading edge to the mid-chord. Image pairs in both planes were taken for 4 s (1.5 s for plasma-off followed by 2.5 s of plasma-on period) at a sample rate of 320 Hz.

The raw images captured by the PIV system were processed by Dantec DynamicStudio 2015a to extract the velocity fields, where the shape and size of the individual interrogation areas (IA) were iteratively adjusted depending on the local seeding densities. The minimum and maximum IAs were limited to 8 and 32 pixels with a 50% overlap, respectively, obtaining around 16000 vectors in each frame. The validation of velocity vectors was made using a universal outlier detection analysis (Westerweel and Scarano, 2005). Any spurious vectors were replaced by a median value calculated using 3 × 3 neighbourhood vectors. Uncertainty in velocity measurements using PIV was estimated by $U_e = \sqrt{\frac{D_e^2}{T^2} + (-\frac{D}{T^2})^2 T_e^2}$ (Kine and McClintock, 1953), assuming that its primary sources of error were the shift distance D of seeding particles and the interval time T between image pairs. Here, D_e is the uncertainty in particle shift distance, which was about 0.15 pixel. The uncertainty in the interval time T_e between image pairs was negligible. This gave $U_e = 0.54$ m/s or $U_e / U_\infty = 5.4\%$, which was similar to the PIV measurements error estimated by Westerweel (1997). Estimated errors of derived quantities, such as the vorticity and circulation, were less than 8% and 10%, respectively.

The plasma actuators were operated either at a steady mode or a pulsed mode at a 50% duty cycle. Here, the normalised pulsed frequency was given by $f^+ = fc/U_\infty$, where f is the modulation frequency, c is the chord length of the wing model and U_∞ is the freestream velocity. Preliminary tests showed that the effective pulsed-mode frequency was $f^+ = 2$, which was identical to that of Sidorenko *et al.* (2013) who examined the flow control on a delta wing. To obtain the momentum coefficient of the plasma jet, PIV measurements of the flow velocity induced by the plasma actuator were conducted without the external flow in a transparent sealed box of 0.6 × 0.3 × 0.3 m^3, which was pre-seeded with tracer particles via a nozzle. We waited 10 minutes before each measurement to make sure that the flow inside was in a quiescent condition. Here, the sample rate and sample duration of the PIV were set to 960 Hz and 3 s, respectively. The momentum coefficient

for the plasma actuators used in this work is shown in Tab. 1. Here, the momentum coefficient of the plasma jet was defined by $C_\mu = M/\frac{1}{2}\rho U_\infty^2 c$, where the momentum flux is given by $M = \int \rho W^2 \mathrm{d}y$ (Jukes and Choi, 2009).

III. RESULTS AND DISCUSSIONS

A. Aerodynamic forces on the very low AR wing with plasma control

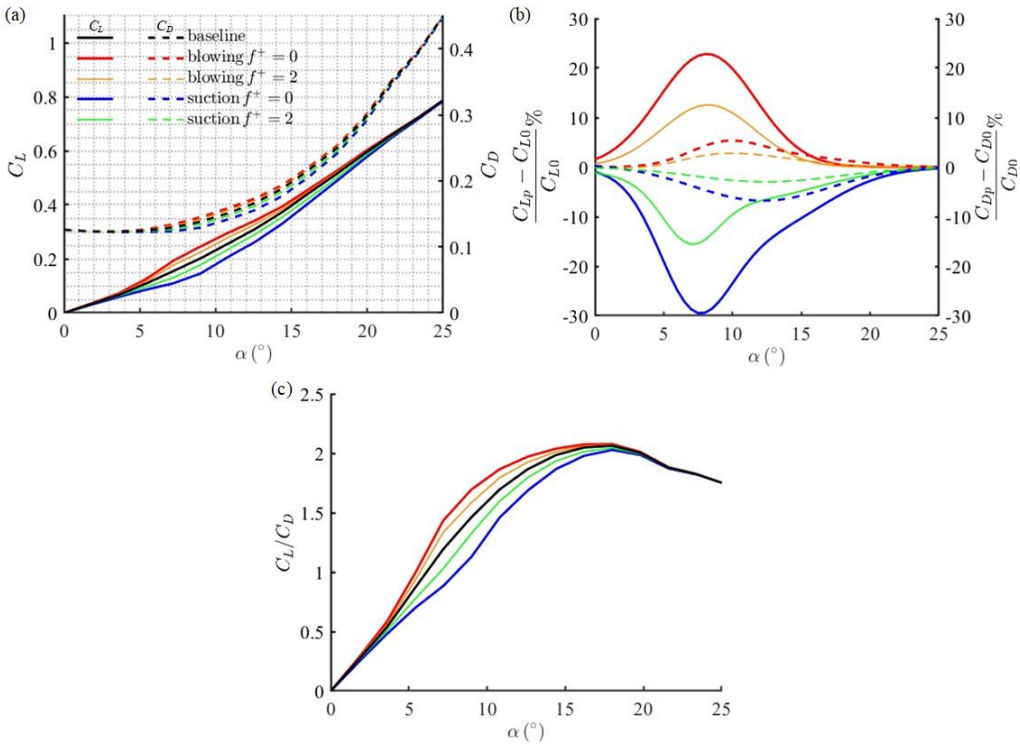

Fig. 4 Effect of the plasma actuators on the aerodynamic forces on a flat-plate wing of the aspect ratio of 0.277 with an elliptic leading edge: (a) C_L and C_D, (b) the increment or decrement of C_L and C_D, (c) lift-to-drag ratio.

The results for lift and drag coefficients with blowing and suction plasma actuators are compared with those of the baseline (plasma off) as shown in Fig. 4a. Here, it should be noted that the aerodynamic forces as well as the flow field around the two baselines, one for the blowing plasma and the other for the suction plasma, were identical within the experimental uncertainties. This clearly shows that the aerodynamic forces are modified by the plasma actuators, where C_L is significantly increased by the blowing plasma actuator but is reduced by the suction plasma actuator between $\alpha = 4°$ and $\alpha = 20°$. Compared to the lift coefficient, the change of the drag coefficient is relatively small with the plasma actuator, which is less than 10% for all cases. The percentage changes in C_L and C_D due to the plasma actuators are shown in Fig. 4b, where the plasma data are indicated by C_{Lp} and C_{Dp}, while the baseline data are given by C_{L0} and C_{D0}, respectively. The most effective control is found at $f^+ = 0$ (steady mode) for both types of plasma actuators. Here, the maximum reduction in C_{L0} can reach 30% by the suction plasma, while the blowing plasma actuator produces an enhancement of C_{L0} by 23%. With a pulsed mode of plasma actuation, the control effect is reduced, where only 16% reduction and 13% enhancement in the lift coefficient are achieved by the suction and blowing plasma at $f^+ = 2$, respectively. This is due to that the plasma momentum coefficient of the steady mode of actuation is about twice that of the pulsed mode of plasma actuation which is operating at 50% of the duty cycle. It is also observed that the most effective control of the plasma on the C_L occurs at around $\alpha = 8°$ for all cases. With a further increase in the AoA, the influence of the plasma actuators gradually vanishes. Figure 4c shows the lift-to-drag ratio of the very low AR wing, which takes the maximum value of $C_L/C_D = 2$ at $\alpha = 18°$. The changes in C_L/C_D as shown in Fig. 4c indicate that the aerodynamic efficiency of the wing can be manipulated by controlling the TV using the plasma actuator. To understand the underlying mechanism of the change in the aerodynamic forces due to plasma control, the behaviour of the TV with plasma at $\alpha = 10°$ and 15° will be demonstrated in the following section.

B. Plasma effect on the TV

The effect of the plasma actuators on the time-averaged, normalised streamwise vorticity ($\omega_x c/U_\infty$) is shown in Fig. 5, where ω_x is the streamwise vorticity, c is the chord length of the wing and U_∞ is the free-stream velocity. Here, the separated flow at the wing tip wraps around from the pressure side to the suction side of the wing, forming a conical-shaped TV stretching along the wing chord. The size and strength of the TV increase downstream with an increase in the AoA. However, there is no sign of the TV breakdown in this figure at least for $0 < x/c < 0.52$ at $\alpha \leq 15°$. A weak, positive vorticity

distribution near the leading edge (x/c < 0.2) is resulted from the interaction of the TV with the LEV, see Yilmaz and Rockwell (2012) at $Re = 1 \times 10^4$ and Dong *et al.* (2022) at $Re = 2 \times 10^5$. Applying the plasma actuators, the streamwise vorticity within the TV core becomes weaker with the suction control and stronger with the blowing control. The diameter of the TV remains unchanged by plasma control, except for suction plasma control ($f^+ = 0$) at $\alpha = 10°$ where a reduction of the TV diameter is clearly seen.

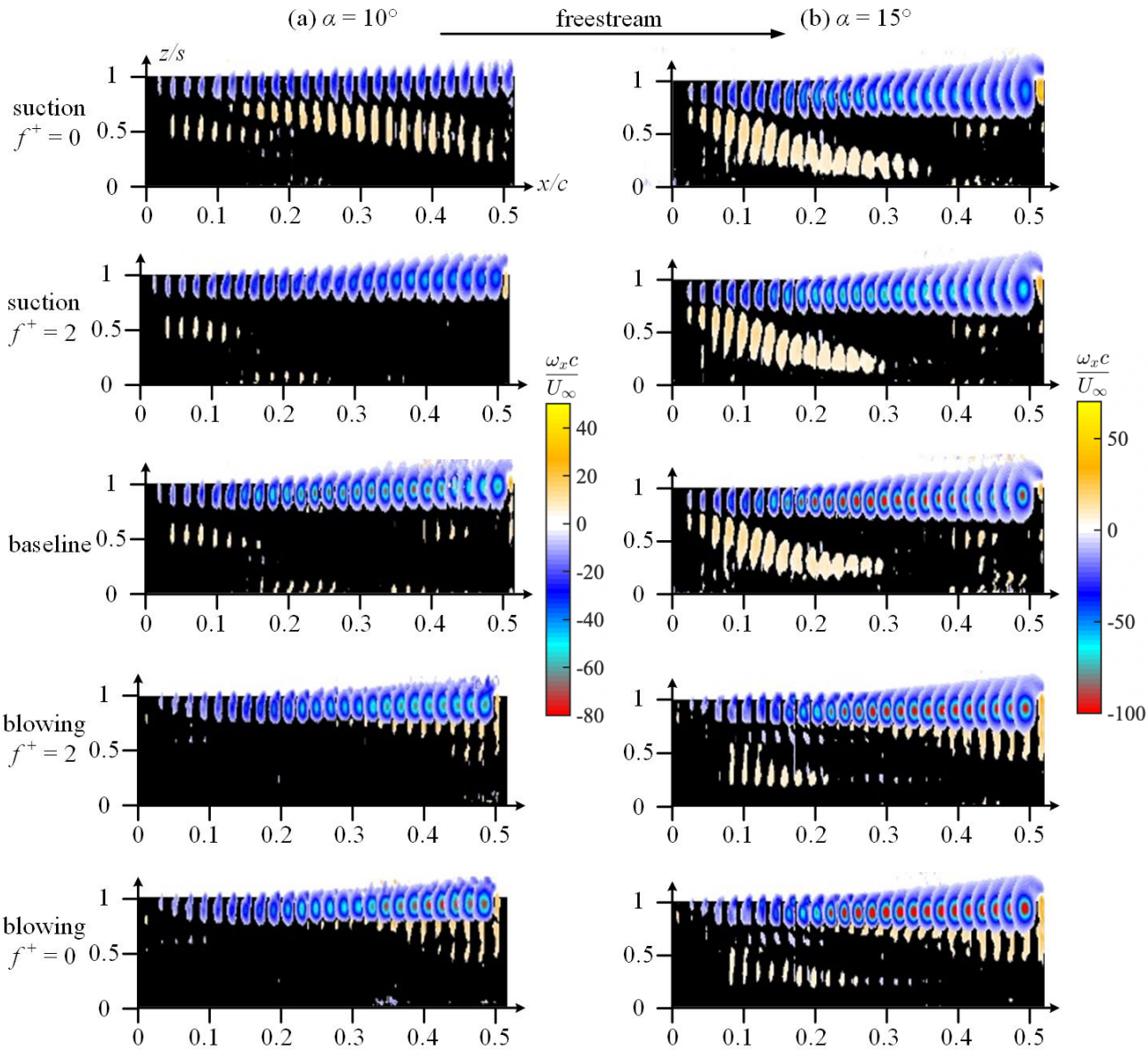

Fig. 5 Side view of the time-averaged, normalised streamwise vorticity ($\omega_x c/U_\infty$) under the influence of the plasma actuators at $\alpha = 10°$ (a) and $\alpha = 15°$ (b) compared with that of the baseline case.

To further examine the influence of the plasma actuators on the TV, the time-averaged vorticity field together with the turbulent intensity and the Reynolds stress distributions at the mid-chord are shown for $\alpha = 10°$ and 15° in Figs. 6 and 7, respectively. Here, the vortex cores, which are indicated by pink circles, are identified by the λ_2-criterion (Jeong and Hussian, 1995), where the corresponding centroids, shown in green dots, are found at the location of the minimum negative value of λ_2. Other vortex identification techniques, including Q-criterion (Chong *et al.,* 1990) and Γ_1–criterion (Graftieaux *et al.*, 2001), give similar results. The TV forms at the wing tip ($z/s = 1$) close to the wing surface, where a weak secondary vorticity is generated, see Fig. 6. The maximum turbulent intensity can be observed in the vortex core around the vortex centroid. The Reynolds stress of the TV exhibits a bi-modal two-lobed distribution.

With suction plasma control at $\alpha = 10°$, see Fig. 6a, the shear layer is forced to move around the wing wall, reducing the flow separation at the wing tip. Particularly when the suction plasma is operated at a steady mode ($f^+ = 0$), the shear layer is reattached to the suction side of the wing surface, creating a small separation bubble. This makes the TV weaker with low vorticity. It is interesting to observe that the turbulent intensity (Fig. 6b) and the Reynolds stress (Fig. 6c) here are increased with the suction plasma. The distribution of the Reynolds stress in the vortex core is no longer bi-modal two-lobed. The strong Reynolds stress appears at the junction of the separated shear layer and the TV, suggesting an enhanced

turbulent mixing there. This is due to a large increase in the *W*-component turbulent intensity, since the *V*-component turbulent intensity is reduced by the suction plasma. For the blowing control, there is no evident movement of the shear layer but the vorticity, turbulent intensity and the Reynolds stress within the TV core are all increased. Here, the increase in the vorticity inside the TV is partly attributed to the added momentum by the blowing plasma jet, which increases the strength of the separated share layer at the wing tip. In addition, the plasma jet velocity is in the same direction as the TV circulation, which helps increase the vorticity as well as the turbulence intensities and the Reynolds stress.

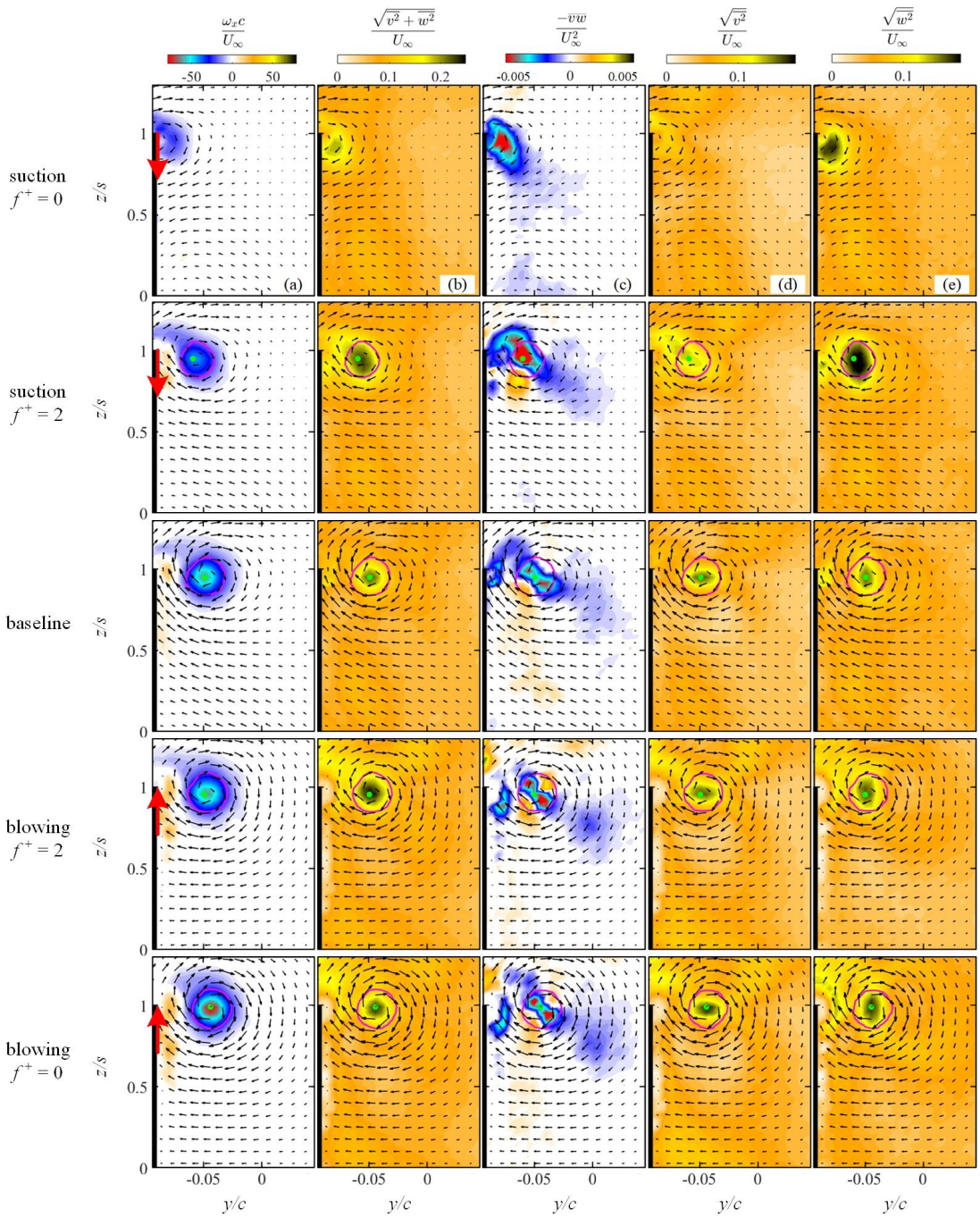

Fig. 6 Influence of the plasma actuators on the TV compared to the baseline case at $\alpha = 10°$ at the mid-chord: (a) the vorticity field, (b) the turbulent intensity, (c) the Reynolds stress, (d) *V*-component turbulent intensity and (e) *W*-component turbulent intensity. Red arrows indicate the location and direction of the plasma jets.

At $\alpha = 15°$ (Fig. 7), the blowing control shows similar results as those at $\alpha = 10°$, by increasing the vorticity, the turbulent intensity and the Reynolds stress within and around the TV core. For the suction control, however, the turbulent intensity and the Reynolds stress are reduced, since both *V*- and *W*-component turbulence intensities are reduced at the same time. We note that the wall-ward movement of the shear layer due to suction is much weaker at $\alpha = 15°$ as compared to the suction control results at $\alpha = 10°$. However, a small separation bubble is still observed near the wing tip with the suction plasma. The suction plasma jet is directed in an opposite direction to the TV circulation, reducing the TV vorticity as well as the turbulence intensities and the Reynolds stress.

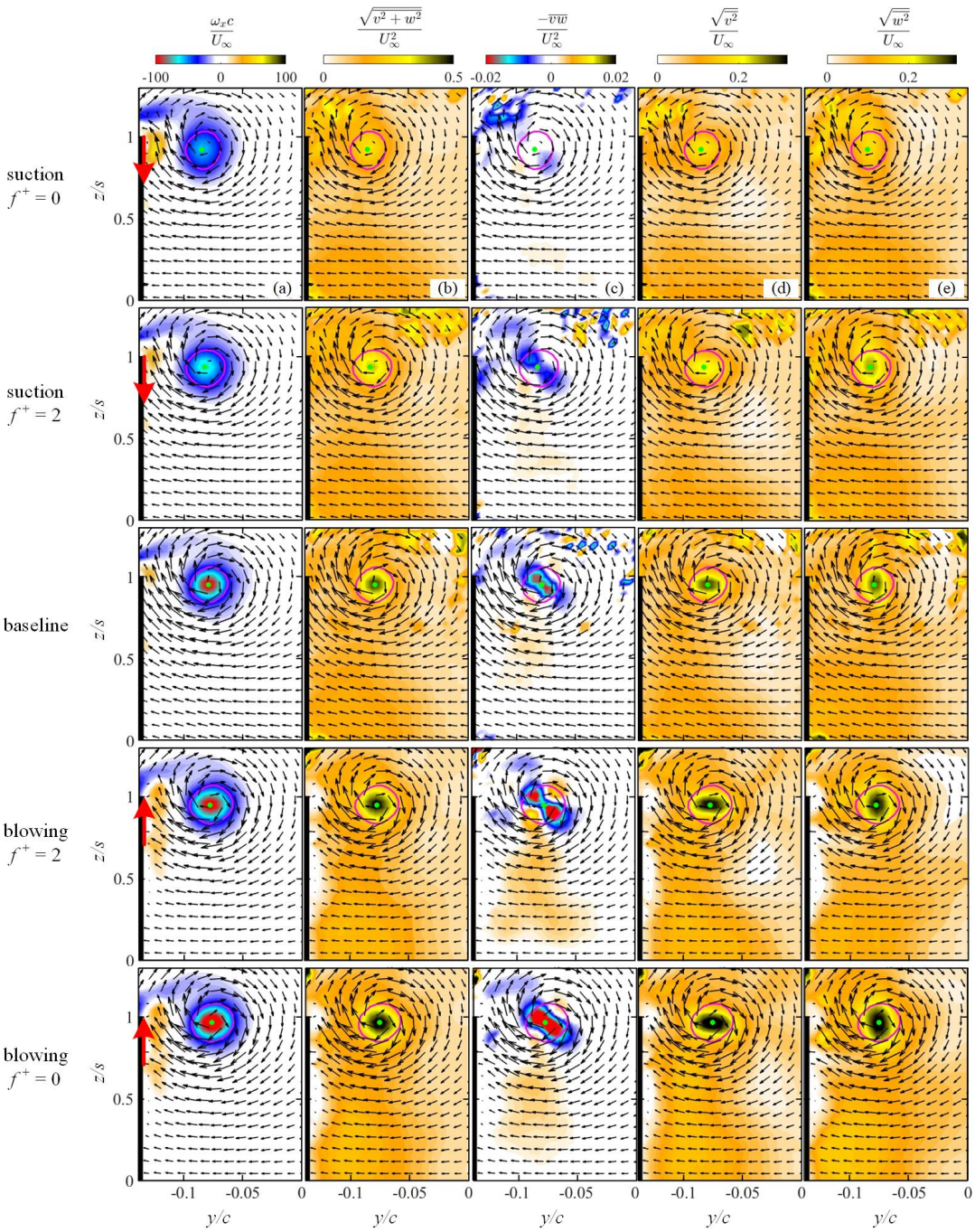

Fig. 7 Influence of the plasma actuators on the TV compared to the baseline case at $\alpha = 15°$ at the mid-chord: (a) the vorticity field, (b) the turbulent intensity, (c) the Reynolds stress, (d) V-component turbulent intensity and (e) W-component turbulent intensity. Red arrows indicate the location and direction of the plasma jets.

Figure 8 shows the locus of the vortex core during the downstream development of the TV in the (y_c/c, z_c/s) plane, where y_c/c and z_c/s are the local non-dimensional coordinates for the vortex core measured from the mid-span and the wing surface, respectively. At $\alpha = 10°$, the locus of the TV core with a steady suction plasma ($f^+ = 0$) remains within $0 < y_c/c < 0.01$ and $0.99 < z_c/c < 1$ (Fig. 8a), as the TV is pulled towards the wing surface to form a separation bubble as shown in Fig. 6a. The TV locus is also shifted towards the wing surface ($y_c/c = 0$) with a pulsed suction plasma ($f^+ = 2$), although a separation bubble is not observed in this case. On the other hand, the vortex core is shifted away from the wing surface as well as from the mid-span by blowing plasma control ($f^+ = 0$ and 2). A similar plasma control behaviour can be observed at $\alpha = 15°$, although the vortex core does not stay near the wing surface with a suction plasma at this AoA.

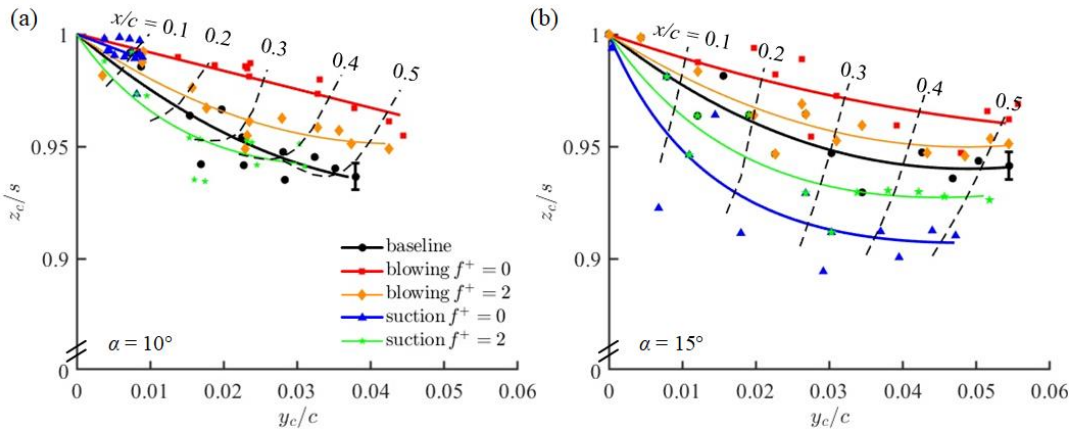

Fig. 8 Change of the vortex locus under the influence of the plasma actuators: (a) $\alpha = 10°$ and (b) $\alpha = 15°$.

The influence of the plasma actuators on the TV circulation along the wing chord is shown by an integral of the vorticity inside the TV core identified by the λ_2-criterion, see Fig. 9. Note that the result for the steady suction plasma actuator has a large uncertainty due to the difficulty in identifying the TV core near the wing surface, see Fig. 6. The circulation of the TV increases nearly linearly with x/c at $\alpha = 10°$, while the linear circulation growth is limited to $x/c < 0.35$ at $\alpha = 15°$. These results are in good agreement with Devoria and Mohseni (2017) at $Re = 8 \times 10^4$ and Dong *et al.* (2022) at $Re = 2 \times 10^5$. As demonstrated in Figs. 6 and 7, the circulation of the TV is reduced by the suction plasma and increased by the blowing plasma. Indeed, suction plasma control of the TV is very effective at $\alpha = 10°$, where the TV circulation is reduced by 75% and 39% at $f^+ = 0$ and 2, respectively, see Fig. 9a. Meanwhile, the increase in the TV circulation by blowing plasma control is 53% and 26% by $f^+ = 0$ and 2, respectively. Increasing AoA to $\alpha = 15°$, the effectiveness of the suction and blowing plasma becomes less but similar to each other with a 33% change (reduction or increase) at $f^+ = 0$ and a 14% change at $f^+ = 2$. A reduction in the control effectiveness of the plasma actuators at $\alpha = 15°$ is due to the reduced velocity ratio of the plasma jet to the W-velocity component of the separated shear layer at the wing tip. While the plasma jet velocity remains constant, the W-velocity component of the separated shear layer is increased with an increase in the AoA.

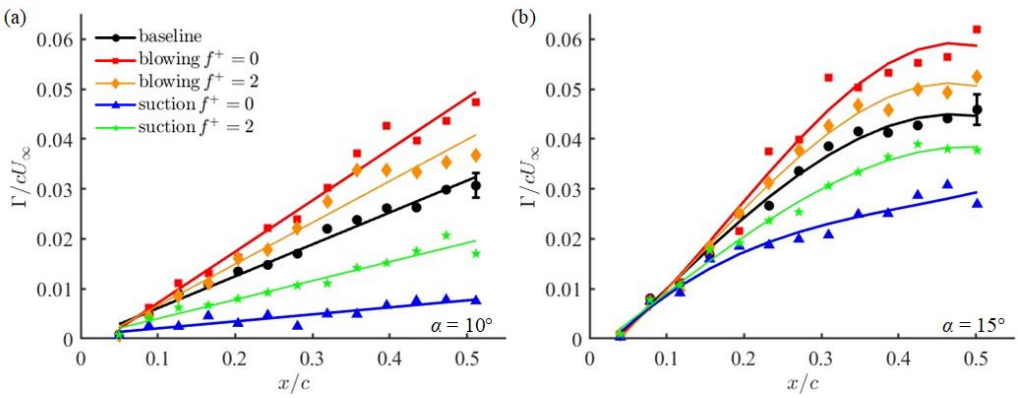

Fig. 9 Effect of the plasma actuators on the TV circulation along the chord at $\alpha = 10°$ (a) and $\alpha = 15°$ (b).

To qualify how the plasma actuator affects the vorticity transport, the time-averaged vorticity flux at the mid-chord ($x/c = 0.5$) is shown in Fig. 10 as a function of y/c. Here, the vorticity flux Ω is defined by $\Omega = -\int \omega_x \sqrt{V^2 + W^2} dz / U_\infty^2$, where the integral of the streamwise vorticity times the local velocity magnitude is performed excluding the contribution of the secondary vorticity between $z/s = 0.75$ and 1.25. A steady suction plasma ($f^+ = 0$) increases the vorticity flux close to the wing surface ($y/c < -0.075$) at $\alpha = 10°$, see Fig. 10a. However, there are only small changes in the vorticity flux due to a pulsed suction plasma ($f^+ = 2$) or the blowing plasma ($f^+ = 0$ and 2) in this region. Away from the wing surface ($y/c > -0.075$), the vorticity flux is reduced by the suction plasma, while it is increased by the blowing plasma. Here, the peak as well as the maximum changes of the vortex flux due to plasma control are found at the centre of the vortex core ($y/c \cong -0.05$). With an increase in the AoA ($\alpha = 15°$), the vorticity flux is increased due to an increase in the streamwise vorticity generated in the separated shear layer as well as the increases in the V- and W-component velocities. Here, there are no appreciable changes in the vorticity flux near the wing surface ($y/c < -0.09$) due to plasma control. Away from the wing surface ($y/c > -0.09$), vortex flux is reduced by the suction plasma ($f^+ = 0$ and 2), while it is increased by the blowing plasma ($f^+ = 0$ and 2). Again, the peak as well as the maximum changes of the vortex flux due to plasma control are found at the centre of the vortex core, which is at $y/c \cong -0.08$ at $\alpha = 15°$.

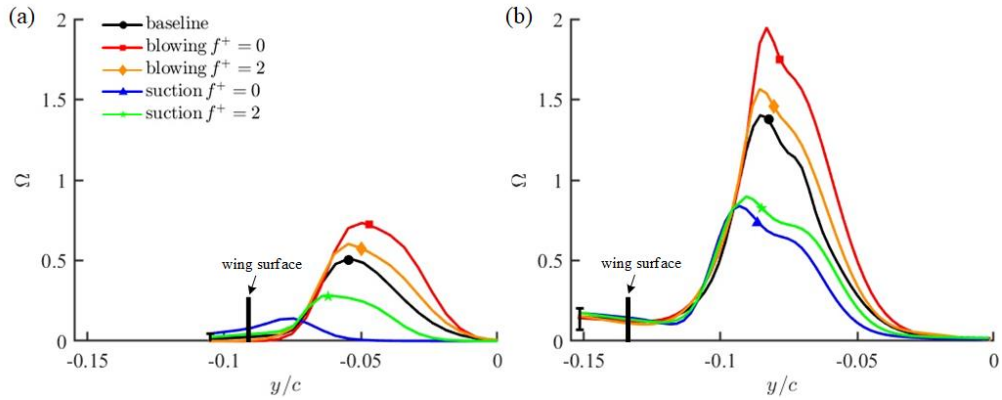

Fig. 10 The vorticity flux Ω between z/s = 0.75 and 1.25 at the mid-chord (x/c = 0.5) at α = 10° (a) and α = 15° (b). Solid symbols on each line indicate the location of the vortex centroid.

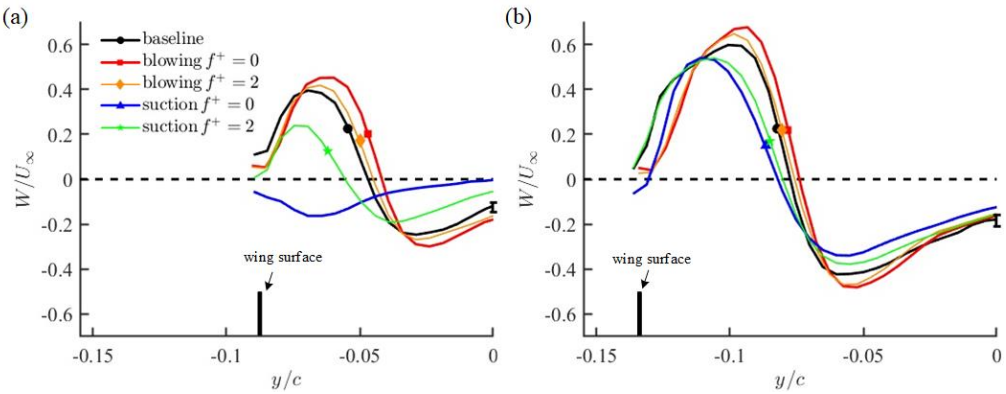

Fig. 11 Effect of the plasma actuators on the W-component velocity of the TV from the wing surface across the vortex centroid at the mid-chord (x/c = 0.5): (a) α = 10° and (b) α = 15°. Solid symbols on each line indicate the location of the vortex centroid.

The W-component velocity distributions across the vortex centroid at the mid-chord (x/c = 0.5) are shown in Fig. 11. Considering that the TV core is located at $y/c \cong$ -0.05 and $y/c \cong$ -0.08 for α = 10° and α = 15°, respectively, the W-component velocity in Fig. 11 represents the circumferential velocity of the TV around the vortex core. With plasma control, the near-wall side of the W-component velocity is increased by the blowing plasma, while it is reduced by the suction plasma. As a result, the TV circulation is increased by blowing control, while it is reduced by suction control. In other words, the blowing plasma increases the TV circulation by co-flowing with the TV, while the TV circulation is reduced by the counter-flowing suction plasma. This suggests that the plasma jet-flow direction relative to the TV circulation is critical in controlling the TVs over a very low AR wing. This seems to be the mechanism of TV circulation control using plasma actuators, which in turn affects the aerodynamic forces of a very low AR wing (Fig. 4). Since the changes in the vorticity flux are only seen away from the wall (Fig. 9), the separated shear layer is not affected by the plasma actuators except for the steady suction plasma (f^+ = 0), where the shear layer is bent over the wing tip to form a separation bubble, see Fig. 6a.

The V-component velocity profiles across the vortex centroid are plotted from the wing tip to the mid-span in Fig. 12, showing the circumferential velocity of the TV. Similar to the W-component velocity which also shows the circumferential velocity of the TV (Fig. 11), the magnitude of the V-component velocity is reduced by suction plasma control, while it is increased by blowing plasma control. It should be noted that the circumferential velocity distribution extends to the mid-span (z/s = 0). Here, the effect of plasma control is seen not only around the vortex core, but also near the mid-span (z/s = 0). In other words, the plasma control can influence the entire flow domain over the wing. It is also noted that the V-component velocity reaches its maximum value closer to the wing tip with the blowing control and to the mid-span with the suction control. The shift of the peak velocity location is due to the movement of the vortex core by plasma control, as demonstrated in Fig. 8.

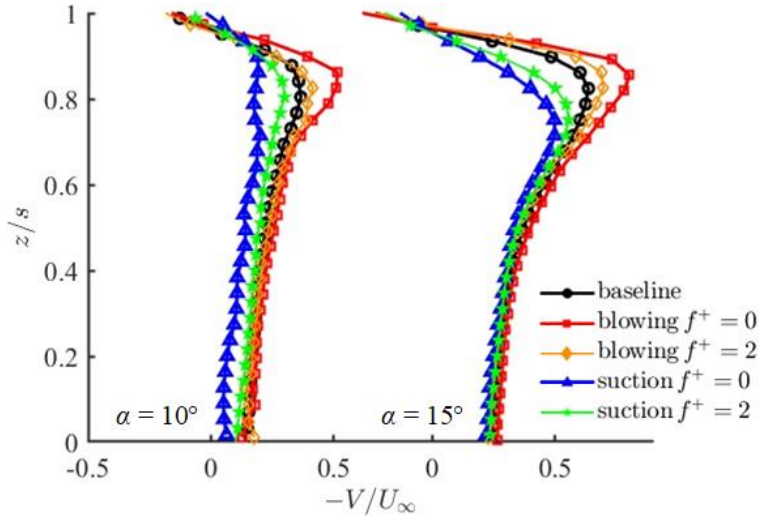

Fig. 12 Effect of the plasma actuators on the V-component velocity from the wing tip across the vortex centroid to the mid-span at the mid-chord ($x/c = 0.5$) with different AoAs.

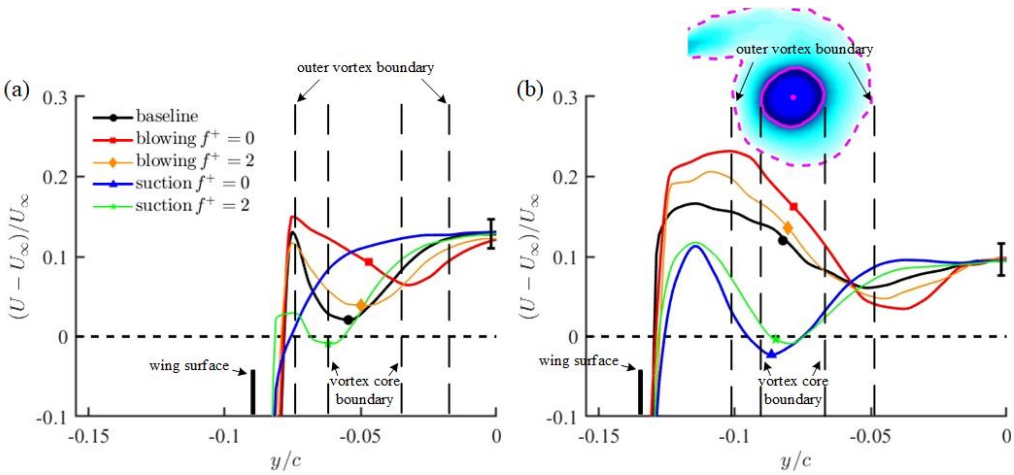

Fig. 13 Effect of the plasma actuators on the U-component velocity of the TV from the wing surface across the vortex centroid at the mid-chord: (a) $\alpha = 10°$ and (b) $\alpha = 15°$. The vortex shown is for the baseline, where outer vortex boundary corresponds to $\omega_x c/U_\infty = -5$. Solid symbols on each line indicate the location of the vortex centroid.

Figure 13 shows the influence of plasma control on the U-component velocity of the TV at $\alpha = 10°$ and $\alpha = 15°$, where the TV centroid and core boundary are marked based on the λ_2-criterion as discussed previously. The vorticity of the TV extends to the outer vortex boundary (Skinner *et al.,* 2020), although the majority is found within the vortex core. Here, the boundary of the outer vortex is defined by the non-dimensional vorticity at $\omega_x c/U_\infty = -5$. The U-component velocity increases sharply from the wing surface and peaks somewhere before entering the outer vortex boundary, which probably is due to the flow acceleration around the wing tip. Thereafter, the U-component velocity reduces inside the TV, followed by a gradual increase, eventually reaching to a final value of around $1.1U_\infty$ outside the outer vortex. When the TV is controlled by a steady suction plasma ($f^+ = 0$) at $\alpha = 10°$, the axial velocity increases monotonically, which is due to the reattachment of the separated shear layer as shown in Fig. 6. The other plasma control cases give a similar velocity profile as the baseline, although the U-component velocity is reduced by the suction plasma and increased by the blowing plasma up to the far-side vortex core boundary at $y/c = -0.05$ at $\alpha = 10°$ and $y/c = -0.056$ at $\alpha = 15°$. Outside the far-side vortex core boundary, the U-component velocity is increased by the suction plasma, while it is reduced by the blowing plasma. The jet-like U-component velocity profiles shown in Fig. 13 seem to suggest that vortex breakdown is not yet taking place at these AoAs. Noteworthy is that the U-component velocity inside the vortex core nearly becomes wake-like by the suction plasma. These results show a possibility that the plasma actuator can also be used to trigger or delay the TV breakdown.

IV. CONCLUDING REMARKS

Flow control of the TVs over a very low AR wing was carried out using the DBD plasma actuators at the effective Reynolds number of 3×10^6, where the steady and pulsed blowing and suction plasma were examined. The results indicate a large change in the aerodynamic forces by plasma flow control, where the lift coefficient is increased by the steady blowing plasma by 23% at the AoA of 8°, while it is reduced by the steady suction plasma by 30%. With a pulsed mode of

plasma actuation, the control effect is reduced, where only a 13% increase and a 16% reduction in the lift coefficient are achieved by the blowing and suction plasma, respectively. This is due to that the plasma momentum coefficient of the steady mode of actuation is about twice that of the pulsed mode of plasma actuation which is operating at 50% of the duty cycle. Compared to the lift coefficient, the change of the drag coefficient is less than 10% for all cases with the plasma actuator. The changes in the aerodynamic forces observed in the present investigation are mainly due to the changes in the vortex lift as a result of the plasma control on the TV circulation. Effect of the plasma actuators on the interaction between LEV and TV is too small to detect since the TV stays very close to the wing tip at the angles of attack being investigated here.

With the blowing plasma the TV moves outboard away from the wing tip, increasing the streamwise vorticity and the turbulence intensities as well as the Reynolds stress. With the suction plasma, the TV is shifted inboard closer to the wing tip. With a steady suction control at $\alpha = 10°$, the separated shear layer is bent around the wing tip, reattaching to the suction side of the wing surface to create a separation bubble. Indeed, the suction plasma is very effective in controlling the TV, reducing the TV circulation by up to 75% at $\alpha = 10°$. Meanwhile, the blowing plasma increases the TV circulation by up to 53%. At $\alpha = 15°$, the effectiveness of the suction and blowing plasma is reduced, which is due to the reduced velocity ratio of the plasma jet to the W-velocity component of the separated shear layer at the wing tip. Co-flowing with the TV, the blowing plasma increases the TV circulation, while it is reduced by the counter-flowing suction plasma. This suggests that the plasma jet-flow direction relative to the TV circulation is critical in controlling the TVs over a very low AR wing. Observed changes in the U-component velocity by plasma control suggests an interesting possibility that the TV breakdown can be manipulated to influence the aerodynamic characteristics.

The main objective of this study is to investigate the TV behaviour in the presence of the plasma actuators and to understand the associated flow control mechanism. This was achieved by dealing with the TV at only one side of the wing. The results indicate that the control effect is isolated to the close vicinity of the wind tip. Therefore, a significant interaction between the two TVs on either side of the wing is unlikely at least at the angles of attack being investigated here. We, therefore, expect that the effect of plasma actuators on the aerodynamics forces on a very low AR wing would be nearly doubled if both wing tips are simultaneously controlled. Although plasma control was carried out on the TVs over a very low AR wing, a similar plasma control strategy can be applied to the leading-edge vortices over the delta wings.

ACKNOWLEDGMENTS

This research was supported by EPSRC (Grant Number EP/N018486/1) in the UK. This project has also received funding from the Clean Sky 2 Joint Undertaking (JU) under grant agreement number 864290. The first author acknowledges the Ph.D. funding provided by the China Scholarship Council (No. 201807000111).

DATA AVAILABILITY

The data that support the findings of this study are available within the article.

REFERENCES

Boesch, G., Vo, H. D., Savard, B., Wanko-Tchatchouang, C., and Mureithi, N. W., "Flight control using wing-tip plasma actuation," J. Aircr. **47**(6), 1836-1846 (2010).

Buchmann, N. A., Atkinson, C., and Soria, J., "Influence of ZNMF jet flow control on the spatio-temporal flow structure over a NACA-0015 airfoil," Exp. Fluids **54**(3), 1-14 (2013).

Chng, T. L., Rachman, A., Tsai, H. M., and Zha, G-C., "Flow control of an airfoil via injection and suction," J. Aircr. **46**(1), 291-300 (2009).

Choi, K-S., Jukes, T. N., Whalley, R. D., Feng, L. H., Wang, J. J., Matsunuma, T., and Segawa, T., "Plasma virtual actuators for flow control," J. Flow Control Meas. Visual. **3**(1), 22 (2015).

Chong, M. S., Perry, A. E., and Cantwell, B. J., "A general classification of three-dimensional flow fields," Phys. Fluids A: Fluid Dyn. **2**(5), 765-777 (1990).

Corke, T. C., Enloe, C. L., and Wilkinson, S. P., "Dielectric barrier discharge plasma actuators for flow control," Annu. Rev. Fluid Mech. **42**, 505-529 (2010).

Corke, T. C., Jumper, E. J., Post, M. L., and Orlov, D., "Application of weakly-ionized plasmas as wing flow-control devices," AIAA paper (2002).

Devenport, W. J., Rife, M. C., Liapis, S. I., and Follin, G. J., "The structure and development of a wing-tip vortex," J. Fluid Mech. **312**, 67-106 (1996).
DeVoria, A. C., and Mohseni, K., "On the mechanism of high-incidence lift generation for steadily translating low-aspect-ratio wings," J. Fluid Mech. **813**, 110-126 (2017).
Dong, L., Choi, K-S., and Mao, X. R., "Interplay of the leading-edge vortex and the tip vortex of a low-aspect-ratio thin wing," Exp. Fluids **61**(9), 1-15 (2020).
Dong, L., Choi, K-S., Mao, X. R., and Wang, Y. X., "Development and interaction of vortices over a very low aspect-ratio wing under pitch-up motion," J. Fluid Mech. **943**, A42 (2022).
Ekaterinaris, J. A., "Prediction of active flow control performance on airfoils and wings," Aerosp. Sci. Technol. **8**(5), 401-410 (2004).
Feng, L. H., Choi, K-S., and Wang, J. J., "Flow control over an airfoil using virtual Gurney flaps," J. Fluid Mech. **767**, 595-626 (2015).
Freymuth, P., "Three-dimensional vortex systems of finite wings," J. Aircr. **25**(10), 971-972 (1988).
Giorgi, M. G. D., Luca, C. G. D., Ficarella, A., and Marra, F., "Comparison between synthetic jets and continuous jets for active flow control: application on a NACA 0015 and a compressor stator cascade," Aerosp. Sci. Technol. **43**, 256-280 (2015).
Giuni, M., "Formation and early development of wingtip vortices," Ph.D. thesis (University of Glasgow, 2013).
Graftieaux, L., Michard M., and Grosjean, N., "Combining PIV, POD and vortex identification algorithms for the study of unsteady turbulent swirling flows," Meas. Sci. Technol. **12**(9), 1422 (2001).
Green S. I., *Springer Science and Business Media* (Fluid vortices, 1995).
Greenblatt, D., Goksel, B., Rechenberg, I., Schule, C. Y., Romann, D., and Paschereit, C. O., "Dielectric barrier discharge flow control at very low flight Reynolds numbers," AIAA J. **46**(6), 1528-1541 (2008).
Harbig, R. R., Sheridan, J., and Thompson, M. C., "Reynolds number and aspect ratio effects on the leading-edge vortex for rotating insect wing planforms," J. Fluid Mech. **717**, 166-192 (2013).
Hasebe, H., Naka, Y., and Fukagata, K., "An attempt for suppression of wing-tip vortex using plasma actuators," J. Fluid Sci. Technol. **6**(6), 976-988 (2011).
He, C., Corke, T. C., and Patel, M. P., "Plasma flaps and slats: an application of weakly ionized plasma actuators," J. Aircr. **46**(3), 864-873 (2009).
Huang, L., Huang, P. G., LeBeau, R. P., and Hauser, T., "Numerical study of blowing and suction control mechanism on NACA0012 airfoil," J. Aircr. **41**(5), 1005-1013 (2004).
Jeong, J., and Hussain, F., "On the identification of a vortex," J. Fluid Mech. **285**, 69-94 (1995).
Kim, J.-H., Choi, K.-S., Lacagnina, G., Chaitanya, P., Joseph, P., Hasheminejad, S. M., Chong, T. P., Shahab, M. F., Omidyeganeh, M., and Pinelli, A., "Aerodynamic and aeroacoustic optimization of leading-edge undulation of a NACA 65(12)-10 airfoil," AIAA J. **60**(4), 2342-2353 (2022).
Kline, S., and McClintock, F., "Describing uncertainties in single-sample experiments," Mech. Engineering **75**, 3–8 (1953).
Kriegseis, J., Simon, B., and Grundmann, S., "Towards in-flight applications? A review on dielectric barrier discharge-based boundary-layer control," Appl. Mech. Rev. **68**(2), 020802 (2016).
Moreau, E., "Airflow control by non-thermal plasma actuators," J. Phys. D: Appl. Phys. **40**(3), 605 (2007).
Post, M. L., and Corke, T. C., "Separation control on high angle of attack airfoil using plasma actuators," AIAA J. **42**(11), 2177-2184 (2004).
Mueller, T. J., "Low Reynolds number vehicles," AGARD AG-288, (1985).
Roth, J. R., "Aerodynamic flow acceleration using paraelectric and peristaltic electrohydrodynamic effects of a one atmosphere uniform glow discharge plasma," Phys. Plasmas **10**(5), 2117-2126 (2003).
Schlichting, H., "Boundary layer theory", McGraw Hill (1955).
Shen, L., and Wen, C-Y., "Leading edge vortex control on a delta wing with dielectric barrier discharge plasma actuators," Appl. Phys. Lett. **110**(25), 251904 (2017).
Sidorenko, A. A., Budovskiy, A. D., Maslov, A. A., Postnikov, B. V., Zanin, B. Y., Zverkov I. D. and Kozlov V. V., "Plasma control of vortex flow on a delta wing at high angles of attack," Exp. Fluids **54**(8), 1-12 (2013).
Skinner, S. N., Green, R. B., and Zare-Behtash, H., "Wingtip vortex structure in the near-field of swept-tapered wings," Phys. Fluids **32**(9), 095102 (2020).
Taira, K., and Colonius, T., "Effect of tip vortices in low-Reynolds-number poststall flow control," AIAA J. **47**(3), 749-756 (2009).
Taira, K., and Colonius, T., "Three-dimensional flows around low-aspect-ratio flat-plate wings at low Reynolds numbers," J. Fluid Mech. **623**, 187-207 (2009).

Torres, G. E., and Mueller, T. J., "Low aspect ratio aerodynamics at low Reynolds numbers," AIAA J. **42**(5), 865-873 (2004).
Vorobiev, A. N., Rennie, R. M., and Jumper, E. J., "Experimental investigation of lift enhancement and roll control using plasma actuators," J. Aircr. **45**(4), 1315-1321 (2008).
Wang, J. J., Choi, K-S. Feng, L. H., Jukes, T. N., and Whalley R. D., "Recent developments in DBD plasma flow control," Prog. Aerosp. Sci. **62**, 52-78 (2013).
Wang, S., Zhou, Y., Alam, M. M., and Yang, H., "Turbulent intensity and Reynolds number effects on an airfoil at low Reynolds numbers," Phys. Fluids **26**(11), 115107 (2014).
Westerweel, J., "Fundamentals of digital particle image velocimetry," Meas. Sci. Technol. **8**(12), 1379-1392 (1997).
Westerweel, J., and Scarano, F., "Universal outlier detection for PIV data," Exp. Fluids **39**(6), 1096-1100 (2005).
Winkelman, A. E., and Barlow, J.B., "Flowfield model for a rectangular planform wing beyond stall," AIAA J. **18**(8), 1006-1008 (1980).
Yilmaz, T. O., and Rockwell, D., "Flow structure on finite-span wings due to pitch-up motion," J. Fluid Mech. **691**, 518-545 (2012).
Zhang, K., Hayostek, S., Amitay, M., He, W., Theofilis, V., and Taira, K., "On the formation of three-dimensional separated flows over wings under tip effects," J. Fluid Mech. **895**, A9 (2020).